Detailed spectroscopy of quadrupole and octupole states in ^{168}Yb

S. Pascu,[1] D. Bucurescu,[1] Gh. Căta-Danil,[1,2] V. Derya,[3] M. Elvers,[3] D. Filipescu,[1] D. G. Ghiţă,[1] T. Glodariu,[1] A. Hennig,[3] C. Mihai,[1] N. Mărginean,[1] R. Mărginean,[1] A. Negret,[1] L. Netterdon,[3] S. G. Pickstone,[3] T. Sava,[1] M. Spieker,[3] L. Stroe,[1] N. V. Zamfir,[1] and A. Zilges[3]

[1]*National Institute for Physics and Nuclear Engineering, R-77125 Bucharest-Magurele, Romania*

[2]*Politehnica Universty of Bucharest, 060042 Bucharest, Romania*

[3]*Institut für Kernphysik, Universität zu Köln, D-50937 Köln, Germany*

(Received 1 October 2014; revised manuscript received 26 February 2015; published 19 March 2015)

The low-lying positive- and negative-parity states in ^{168}Yb have been investigated by means of the $(\alpha,2n\gamma)$ fusion evaporation reaction. Using the coincidence method, the level scheme was corrected and extended up to 3 MeV, for both the positive- and negative-parity states. Using the new branching ratios determined in the present experiment, the K quantum number was proposed for two negative-parity bands by direct comparison with the Alaga rule. Like in some other nuclei, one negative-parity band was established, decaying predominantly to the γ-vibrational band. In a second experiment, the lifetimes of the low-lying excited states up to $J^\pi = 6^+$ in the ground-state band were measured by using the in-beam fast-timing method with the Bucharest mixed high-purity germanium (HPGe) and $LaBr_3$:Ce detector array using the triple-γ coincidence method. Reduced $E2$ transition probabilities were extracted from the measured lifetimes and compared with the corresponding observables in neighboring isotopes, showing a smooth behavior with increasing mass. The positive- and negative-parity states as well as $E1$ and $E2$ transition probability ratios revealed by these experiments are compared with the interacting boson model in the sd and $spdf$ boson space, and with the confined beta-soft rotor model, and are found to be in good agreement.

DOI: 10.1103/PhysRevC.91.034321 PACS number(s): 21.10.−k, 21.60.Ev, 23.20.Js, 27.70.+q

I. INTRODUCTION

The Yb isotopes around mass 170 are known to exhibit rotational properties. Having the ratio between the energy of the first 4^+ state and the energy of the first 2^+ state ($R_{4/2}$ ratio) of 3.27 (close to the rotational limit of 3.33) ^{168}Yb should display most of the characteristic features of an axial rotor. The structure of this nucleus has been intensively investigated in recent years using a wide range of experimental methods—including β-decay studies [1–3], heavy ion reactions [4–6], transfer reactions [7,8], Coulomb excitation [9], and neutron-induced reactions [10]—establishing several band structures such as the β- and γ-vibrational bands. These studies mostly concentrated on investigating the positive-parity states at low and medium spins. Various nuclear structure models have been employed to explain the structure of this nucleus and its neighboring isotopes, such as the interacting boson model (IBM) with different types of bosons [11–14], the interacting vector boson model [15], and the quasiparticle random phase approximation [16]. High-spin states have also been studied [5,17] and interpreted in the framework of the angular momentum projected Tamm-Dancoff approximation [18]. However, the low-lying negative-parity states have not received the same attention and therefore no band structure with negative-parity has been constructed so far. The same situation is found also with respect to the $E1$ and $E2$ reduced transition probabilities, where very sparse information is found [19]. Therefore, the goal of these experiments was twofold: first to establish band structures in order to derive the K quantum numbers and second to measure the lifetimes of the positive-parity states and compare the extracted information with the adjacent nuclei. A well-known reaction suited to populate excited states at low and medium spins in atomic nuclei is the $(\alpha,2n)$ reaction at moderate energies. Therefore, the ^{166}Er$(\alpha,2n\gamma)^{168}$Yb reaction was selected. This reaction was already used in several previous experiments [20,21], where the authors concentrated on populating higher spins; therefore the energy chosen for these studies was higher than in the present experiments. Our studies revealed in the first step new energy levels and γ-ray transitions especially in the β-vibrational band. Furthermore, the K quantum numbers for two octupole-vibrational bands were assigned by comparison with the Alaga rule. In a second step, the lifetimes of the low-lying excited states up to the 6^+ state in the ground-state band were measured by using the in-beam fast-timing method. The experimental setups and the details of both experiments for constructing the level scheme and for lifetime measurements are discussed in Sec. II, while in Sec. III a theoretical interpretation of the observed quantities is given in terms of band-mixing and is compared with calculations performed within the interacting boson model and the confined beta-soft (CBS) rotor model.

II. EXPERIMENTAL DETAILS AND RESULTS

A. Determination of new energy levels and γ-ray transitions

The nucleus ^{168}Yb was produced by bombarding a 97% self-supporting enriched ^{166}Er target of 2 mg/cm^2 thickness with 25.5 MeV α particles from the 10 MV tandem accelerator in Cologne. The experiment was conducted with an average 2.5 pnA cup current using the HORUS setup. This spectrometer consists of 14 high-purity germanium (HPGe) detectors providing a high efficiency of about 2% at 1332 keV. In the present experiment only 13 detectors were available. All HPGe detectors were energy calibrated and the relative efficiency

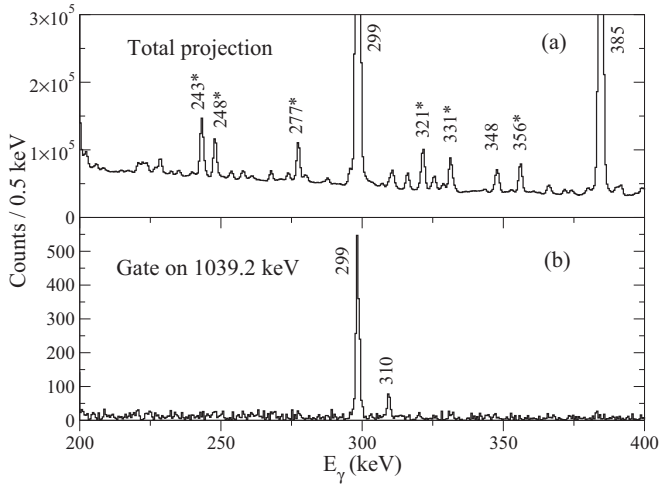

FIG. 1. Sample γ-ray spectra from the ^{166}Er(α,2n) reaction. (a) Total projection spectrum of a symmetric γ-γ coincidence matrix; (b) projection of the γ-γ matrix gated by the 1039.2 keV γ ray ($6^+_\beta \rightarrow 6^+_1$). The newly observed peak at 310 keV corresponds to an intraband transition in the β-vibrational band which was selected from a region where multiple γ rays belonging to ^{169}Yb are present [marked with asterisk in panel (a)].

was determined using a ^{226}Ra source. Double- and higher-fold coincidences between all these detectors were registered online and sorted to coincidence matrices after the experiment. Figure 1 shows two examples of γ-ray spectra recorded in this experiment. Panel (a) presents a total projection spectrum of a symmetric γ-ray matrix, while the spectrum in panel (b) shows the power of γ-γ coincidence measurements in revealing weak transitions. The spectrum presents a weak transition at 310 keV which is newly assigned in this experiment as resulting from the decay of the proposed 8^+ state of the β band at 1933.9 keV.

Using the coincidence technique, the level scheme of ^{168}Yb was extended and corrected. In total, 151 transitions were assigned and 28 new levels up to an excitation energy of 3 MeV were identified. The spin transfer was rather high and consequently the high-spin states were observed up to 14^+. However, the octupole band heads were not excited but several possible members of the octupole band with higher spins were found and new transitions for the known octupole states were determined. Additionally, new energy levels that are candidates for being members of the previously assigned β- and γ-vibrational bands were found. The complete set of results is presented in Table I, while the states assigned to various positive- or negative-parity bands in previous studies or the present work are presented in Fig. 2 and will be discussed in detail in Sect. III.

B. Lifetime measurement experiment

In this section we report on a measurement of lifetimes for several excited levels in the ground-state band of ^{168}Yb. The experiment employed the new in-beam fast-timing method suited for measuring lifetimes of nuclear states in the nanosecond region described in Ref. [22]. Excited states in ^{168}Yb were populated using the ^{166}Er(α,2nγ)^{168}Yb reaction. The α beam was accelerated to 24 MeV by the 9 MV tandem accelerator of the National Institute of Physics and Nuclear Engineering from Bucharest, and impinged on a 2 mg/cm^2 enriched ^{166}Er self-supported target. The average beam intensity on target was about 3 pnA.

The detection of the γ rays produced in the reaction was done with a mixed array of 8 HPGe detectors and 11 $LaBr_3$:Ce scintillators placed around the target chamber. The HPGe detectors had a relative efficiency of 50%; five of them were placed at backward angles of 143°, two at 90°, and one at 30° with respect to the beam direction. The $LaBr_3$:Ce detectors had various crystal dimensions, 2 in. × 2 in., 1.5 in. × 1.5 in. cylindrical crystals, and 1 in. × 1.5 in. × 1.5 in. of conical shape. This corresponds to a detection efficiency of about 1% for the HPGe detectors and 1% for the $LaBr_3$:Ce detectors at $E_\gamma = 1.33$ MeV. Data were recorded by requesting a threefold coincidence, namely that γ rays were observed in $\geqslant 2$ $LaBr_3$:Ce detectors and $\geqslant 1$ HPGe detector.

The HPGe and $LaBr_3$:Ce detectors were calibrated in energy using ^{152}Eu and ^{60}Co standard sources. Because of the gain instability of the $LaBr_3$:Ce photomultipliers caused by the count rate fluctuations, a run-by-run gain matching procedure was applied. The energy dependence of the time response is treated as in Ref. [22] by using a ^{60}Co source and placing a gate on the 1332 keV transition in the reference

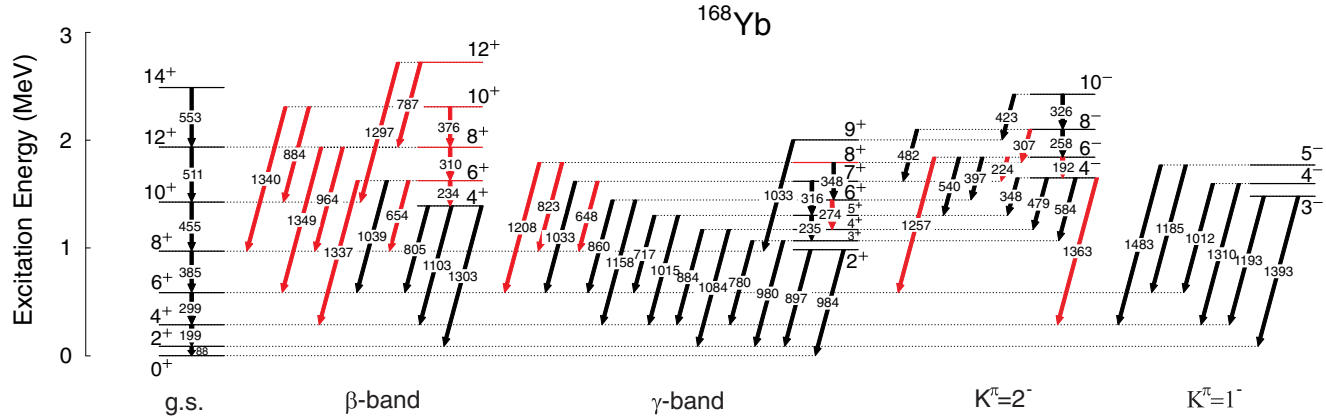

FIG. 2. (Color online) Part of the level scheme for ^{168}Yb. New transitions and levels are in red.

TABLE I. States in ^{168}Yb up to 3 MeV and their γ decays observed in the present experiment. The state energy E, the initial and final spin and K quantum number $J^{\pi}_{i,f}$ and $K^{\pi}_{i,f}$, the final energy E_f, the energy of the γ ray E_γ, and the branching ratios (normalized to the most intense γ ray for each level) I_γ are listed. The uncertainties of the transition energies are below 1 keV. Newly assigned states and transitions are labeled with a.

E (keV)	K^{π}_i	J^{π}_i		J^{π}_f	K^{π}_f	E_f (keV)	E_γ (keV)	I_γ
87.73(1)	0^+_1	2^+	$\rightarrow$	0^+	0^+_1	0.00	87.73	100
286.55(2)	0^+_1	4^+	$\rightarrow$	2^+	0^+_1	87.73(1)	198.84	100
585.25(5)	0^+_1	6^+	$\rightarrow$	4^+	0^+_1	286.55(2)	298.74	100
970.02(11)	0^+_1	8^+	$\rightarrow$	6^+	0^+_1	585.25(5)	384.75	100
983.60(20)	2^+_γ	2^+	$\rightarrow$	2^+	0^+_1	87.73(1)	895.85	100(8)
				0^+	0^+_1	0.0	983.60	80(8)
1066.64(20)	2^+_γ	$(3)^+$	$\rightarrow$	4^+	0^+_1	286.55(2)	780.08	23.2(20)
				2^+	0^+_1	87.73(1)	978.93	100(6)
1170.86(20)	2^+_γ	(4^+)	$\rightarrow$	4^+	0^+_1	286.55(2)	884.28	100(8)
				2^+	0^+_1	87.73(1)	1083.15	45(5)
1301.95(22)	2^+_γ	(5^+)	$\rightarrow$	$(3)^+$	2^+_γ	1066.64(20)	235.27	3.1(6)
				6^+	0^+_1	585.25(5)	716.80	23.1(21)
				4^+	0^+_1	286.55(2)	1015.32	100(7)
1390.03(21)	0^+_β	4^+	$\rightarrow$	6^+	0^+_1	585.25(5)	804.86	31(13)
				4^+	0^+_1	286.55(2)	1103.45	95(45)
				2^+	0^+_1	87.73(1)	1302.24	100(36)
1425.41(22)	0^+_1	10^+	$\rightarrow$	8^+	0^+_1	970.02(11)	455.40	100
1445.00(22)	2^+_γ	$(6)^+$	$\rightarrow$	(4^+)	2^+_γ	1170.86(20)	274.17[a]	14(4)
				6^+	0^+_1	585.25(5)	859.81	100(12)
				4^+	0^+_1	286.55(2)	1158.35	49(9)
1451.40(21)	3^+	$(3)^+$	$\rightarrow$	2^+	2^+_γ	983.60(20)	467.76	36(5)
				4^+	0^+_1	286.55(2)	1164.91	23(4)
				2^+	0^+_1	87.73(1)	1363.65	100(10)
1479.60(21)	1^-	3^-	$\rightarrow$	4^+	0^+_1	286.55(2)	1193.09	76(52)
				2^+	0^+_1	87.73(1)	1391.83	100(46)
1551.14(33)	3^+	4^+	$\rightarrow$	$(3)^+$	3^+	1451.40(21)	99.99	22(6)
				(4^+)	2^+_γ	1170.86(20)	379.98	84(27)
				$(3)^+$	2^+_γ	1066.64(20)	484.79	22(7)
				4^+	0^+_1	286.55(2)	1264.39	100(18)
				2^+	0^+_1	87.73(1)	1463.36	72(19)
1597.32(32)	1^-	$(4)^-$	$\rightarrow$	6^+	0^+_1	585.25(5)	1012.26	57(13)
				4^+	0^+_1	286.55(2)	1310.85	100(14)
1618.32(23)	2^+_γ	(7^+)	$\rightarrow$	(5^+)	2^+_γ	1301.95(22)	316.29	23.5(19)
				8^+	0^+_1	970.02(11)	648.42[a]	21.1(19)
				6^+	0^+_1	585.25(5)	1033.02	100(7)
1624.33(22)[a]	0^+_β	(6^+)	$\rightarrow$	4^+	0^+_β	1390.03(21)	234.26[a]	6.4(23)
				8^+	0^+_1	970.02(11)	654.21[a]	17(5)
				6^+	0^+_1	585.25(5)	1039.19[a]	46(8)
				4^+	0^+_1	286.55(2)	1337.81[a]	100(10)
1650.19(25)	2^-	$(4)^-$	$\rightarrow$	(5^+)	2^+_γ	1301.95(22)	348.27	63(5)
				(4^+)	2^+_γ	1170.86(20)	479.25	35(3)
				$(3)^+$	2^+_γ	1066.64(20)	583.41	100(7)
				4^+	0^+_1	286.55(2)	1363.82[a]	5.4(15)
1673.95(33)	3^+	(5^+)	$\rightarrow$	4^+	3^+	1551.14(33)	123.29	11.3(15)
				$(3)^+$	3^+	1451.40(21)	222.66	19.5(23)
				(5^+)	2^+_γ	1301.95(22)	371.78	24(3)
				$(3)^+$	2^+_γ	1066.64(20)	607.13[a]	26(4)
				6^+	0^+_1	585.25(5)	1088.63	29(4)
				4^+	0^+_1	286.55(2)	1387.27	100(9)
1764.74(37)[a]		(4,5,6)	$\rightarrow$	6^+	0^+_1	585.25(5)	1179.28[a]	100(7)
				4^+	0^+_1	286.55(2)	1478.41[a]	25(3)
1769.84(30)	1^-	5^-	$\rightarrow$	(4^+)	2^+_γ	1170.86(20)	598.72[a]	5.3(20)
				6^+	0^+_1	585.25(5)	1184.74	53(4)
				4^+	0^+_1	286.55(2)	1483.39	100(7)

TABLE I. (*Continued.*)

E (keV)	K_i^π	J_i^π		J_f^π	K_f^π	E_f (keV)	E_γ (keV)	I_γ
1790.29(84)[a]		(8,9,10)	→	10^+	0_1^+	1425.41(22)	776.31[a]	100(7)
				8^+	0_1^+	970.02(11)	408.85[a]	67(5)
1792.82(21)[a]	2_γ^+	(8^+)	→	$(6)^+$	2_γ^+	1445.00(22)	347.88[a]	29(4)
				8^+	0_1^+	970.02(11)	822.77[a]	100(12)
				6^+	0_1^+	585.25(5)	1207.53[a]	51(12)
1800.38(22)[a]		(6,7,8)	→	8^+	0_1^+	970.02(11)	830.42[a]	28.3(22)
				6^+	0_1^+	585.25(5)	1215.07[a]	100(6)
1819.05(34)	3^+	(6^+)	→	(5^+)	3^+	1673.95(33)	145.54	69(10)
				4^+	3^+	1551.14(33)	268.01	100(10)
				$(6)^+$	2_γ^+	1445.00(22)	373.88	33(7)
				6^+	0_1^+	585.25(5)	1233.69	76(20)
				4^+	0_1^+	286.55(2)	1532.28	55(13)
1842.08(30)	2^-	(6^-)	→	$(4)^-$	2^-	1650.19(25)	191.86[a]	7(4)
				(7^+)	2_γ^+	1618.32(23)	224.01[a]	12(3)
				$(6)^+$	2_γ^+	1445.00(22)	397.03	18(4)
				(5^+)	2_γ^+	1301.95(22)	539.82	100(9)
				6^+	0_1^+	585.25(5)	1257.01[a]	22(6)
1933.94(30)[a]	0_β^+	(8^+)	→	(6^+)	0_β^+	1624.33(22)	309.62[a]	21(4)
				8^+	0_1^+	970.02(11)	964.15[a]	55(9)
				6^+	0_1^+	585.25(5)	1348.47[a]	100(12)
1936.00(50)	0_1^+	12^+	→	10^+	0_1^+	1425.41(22)	510.50	100
1972.15(20)[a]			→	4^+	0_1^+	286.55(2)	1685.59[a]	100(8)
				$(4)^-$	1^-	1597.32(32)	374.83[a]	7.6(19)
1985.03(50)	3^+	(7^+)	→	(6^+)	3^+	1819.05(34)	166.48	34(6)
				(5^+)	3^+	1673.95(33)	310.71	58(8)
				(7^+)	2_γ^+	1618.32(23)	366.57[a]	100(10)
1998.66(35)	$\geqslant 2$	5^-	→	(6^-)	2^-	1842.08(30)	156.88	41(6)
				(6^+)	3^+	1819.05(34)	179.98	45(7)
				5^-	1^-	1769.84(30)	228.62	100(10)
				(5^+)	3^+	1673.95(33)	324.78	42(7)
				$(4)^-$	2^-	1650.19(25)	348.19	92(12)
				$(4)^-$	1^-	1597.32(32)	400.99	33(6)
				6^+	0_1^+	585.25(5)	1413.47	27(7)
2002.65(20)	2_γ^+	(9^+)	→	8^+	0_1^+	970.02(11)	1032.63	100
2031.50(23)[a]		(4,5,6)	→	(4^+)	2_γ^+	1170.86(20)	860.54[a]	100(8)
				(5^+)	2_γ^+	1301.95(22)	729.53[a]	98(8)
				6^+	0_1^+	585.25(5)	1446.38[a]	10.0(21)
2050.77(33)[a]			→	3^-	1^-	1479.60(21)	570.99[a]	62(23)
				4^+	0_1^+	286.55(2)	1764.41[a]	100(34)
2055.45(30)		$(2^+,3^+,4^+)$	→	$(3)^+$	2_γ^+	1066.64(20)	988.97	58(13)
				2^+	2_γ^+	983.60(20)	1071.69	100(14)
2083.05(20)[a]		(8,9,10)	→	10^+	0_1^+	1425.41(22)	657.62[a]	16.1(13)
				8^+	0_1^+	970.02(11)	1113.04[a]	100(6)
2088.09(20)[a]		(6,7,8)	→	8^+	0_1^+	970.02(11)	1118.09[a]	100(7)
				6^+	0_1^+	585.25(5)	1502.83[a]	18(3)
2100.03(30)	2^-	(8^-)	→	(6^-)	2^-	1842.08(30)	258.09	20.1(19)
				(8^+)	2_γ^+	1792.82(21)	307.33[a]	5.0(13)
				(7^+)	2_γ^+	1618.32(23)	481.46	100(7)
2100.72(28)[a]		(4,5,6)	→	6^+	0_1^+	585.25(5)	1515.62[a]	100(13)
				4^+	0_1^+	286.55(2)	1814.02[a]	48(8)
2110.94(20)	$\geqslant 2$	$(5,6,7)^-$	→	5^-	$\geqslant 2^-$	1998.66(35)	112.28	100(10)
				4^+	0_1^+	286.55(2)	1524.97	0.6(3)
2160.35(33)[a]		(8,9,10)	→	10^+	0_1^+	1425.41(22)	734.75[a]	21.3(23)
				8^+	0_1^+	970.02(11)	1190.52[a]	100(8)
2172.00(20)[a]		(8^+)	→	(6^+)	3^+	1819.05(34)	352.96[a]	4.7(16)
				10^+	0_1^+	1425.41(22)	746.56[a]	5.1(10)
				8^+	0_1^+	970.02(11)	1201.98[a]	100(7)

TABLE I. (*Continued.*)

E (keV)	K_i^π	J_i^π		J_f^π	K_f^π	E_f (keV)	E_γ (keV)	I_γ
2174.59(26)[a]		(4,5,6)	→	$(4)^-$	1^-	1597.32(32)	577.14[a]	99(21)
				(6^-)	2^-	1842.08(30)	332.70[a]	28(8)
				5^-	1^-	1769.84(30)	404.69[a]	100(16)
2178.07(20)[a]		(4,5,6)	→	$(4)^-$	1^-	1597.32(32)	580.76[a]	100(14)
				(6^-)	2^-	1842.08(30)	335.98[a]	15(5)
2178.85(20)[a]		(6,7,8)	→	8^+	0_1^+	970.02(11)	1208.86[a]	22(4)
				6^+	0_1^+	585.25(5)	1593.57[a]	100(15)
2223.22(20)		$(^-)$	→	$(5,6,7)^-$	$\geqslant 2^-$	2110.94(20)	112.28	100(10)
				5^-	$\geqslant 2^-$	1998.66(35)	223.71	11(6)
2300.92(32)[a]		(8,9,10)	→	10^+	0_1^+	1425.41(22)	875.33[a]	28(3)
				8^+	0_1^+	970.02(11)	1331.08[a]	100(8)
2309.76(33)[a]	0_β^+	(10^+)	→	(8^+)	0_β^+	1933.94(30)	375.66[a]	27(6)
				10^+	0_1^+	1425.41(22)	884.20[a]	100(8)
				8^+	0_1^+	970.02(11)	1340.05[a]	85(9)
2326.55(41)[a]		(6,7,8)	→	8^+	0_1^+	970.02(11)	1356.28[a]	32(8)
				6^+	0_1^+	585.25(5)	1741.55[a]	100(13)
2339.62(70)[a]		(6,7,8)	→	8^+	0_1^+	970.02(11)	1369.12[a]	81(14)
				6^+	0_1^+	585.25(5)	1754.84[a]	100(13)
2395.06(28)[a]		(8,9,10)	→	10^+	0_1^+	1425.41(22)	969.51[a]	100(7)
				8^+	0_1^+	970.02(11)	1425.18[a]	35(4)
2424.65(47)[a]		(8^+)	→	10^+	0_1^+	1425.41(22)	999.60[a]	100(11)
				8^+	0_1^+	970.02(11)	1454.17[a]	50(11)
				6^+	0_1^+	585.25(5)	1839.49[a]	55(13)
2425.99(27)	2^-	(10^-)	→	(8^-)	2^-	2100.03(30)	325.83	100(8)
				(9^+)	2_γ^+	2002.65(20)	423.46	71(8)
2482.84(21)[a]			→	(8^+)	2_γ^+	1792.82(21)	689.98[a]	30(6)
				8^+	0_1^+	970.02(11)	1512.86[a]	100(10)
2488.62(20)	0_1^+	(14^+)	→	12^+	0_1^+	1936.00(50)	552.62	100
2508.58(20)[a]		(6,7,8)	→	8^+	0_1^+	970.02(11)	1538.54[a]	100(14)
				6^+	0_1^+	585.25(5)	1923.35[a]	42(11)
2535.74(39)[a]		(6,7,8)	→	8^+	0_1^+	970.02(11)	1565.95[a]	100(10)
				6^+	0_1^+	585.25(5)	1950.25[a]	67(11)
2558.32(28)[a]		(6,7,8)	→	8^+	0_1^+	970.02(11)	1588.16[a]	100(17)
				6^+	0_1^+	585.25(5)	1973.21[a]	41(10)
2605.68(21)[a]			→	8^+	0_1^+	970.02(11)	1635.63[a]	100(11)
				(8^-)	2^-	2100.03(30)	505.68[a]	19(4)
2722.59(28)[a]	0_β^+	(12^+)	→	12^+	0_1^+	1936.00(50)	786.45[a]	90(16)
				10^+	0_1^+	1425.41(22)	1297.32[a]	100(10)
2846.19(120)		(13^-)	→	12^+	0_1^+	1936.00(50)	910.19	100
2930.00(39)		(13^+)	→	(11^+)		2442.87(40)	487.47	100(7)
				12^+	0_1^+	1936.00(50)	993.85	23(4)

[a]Observed for the first time.

detector. In this way one obtains the response of the CFD for all energies smaller than 1173 keV, which can be fitted with a polynomial function and corrected offline. However, for energies smaller than ∼200 keV the presence of the backscattered events prevents the use of the ^{60}Co source for the walk correction. To properly characterize the time-walk response below this energy range, the authors of Ref. [23] have performed the correction by analyzing the prompt response difference within the mirror symmetric centroid difference method by using different calibration sources, e.g., ^{133}Ba. In the present experiment, an even more precise internal correction was applied to obtain the lifetime of the 6^+ state in the ground-state band by using the data from the present reaction itself. By employing this method a gate on the 455 keV γ ray deexciting the 10^+ state in the ground-state band was placed and the electronic shift for all available energies (γ rays in the ground-state band below 10^+) was observed. The lifetime of these states which were used for the time-walk correction is either assumed to be negligible for the fast-timing method (e.g., the lifetime of the 8^+ state) or it was determined using the deconvolution method (the lifetimes of the 2^+ and 4^+ states) which will be briefly explained. We have estimated that this walk-correction method will introduce an additional systematic uncertainty of the order of 1–2 ps. This value is negligible for most of the lifetimes that can be determined by the fast-timing method, but for the small lifetime of the 6^+

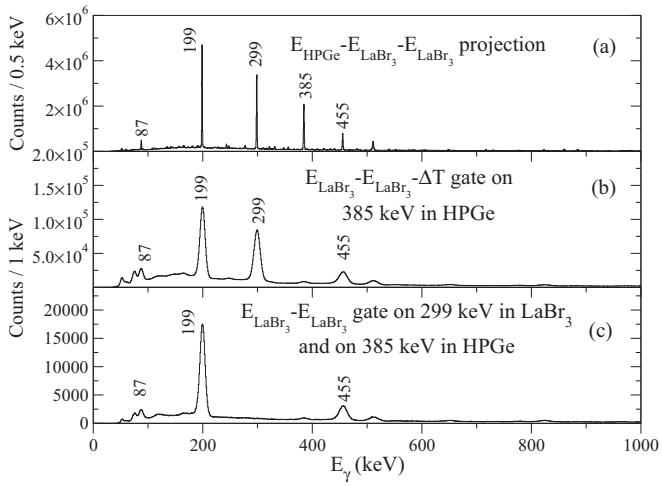

FIG. 3. (a) Projection to the HPGe axis of a $\gamma\gamma\gamma$ (E_{HPGe}-E_{LaBr_3}-E_{LaBr_3}) coincidence cube. (b) Projection to the energy (γ rays observed in the $LaBr_3$:Ce detectors) axis of the $E_{\gamma 1}$-$E_{\gamma 2}$-ΔT cube gated by the 385 keV γ ray in the HPGe detectors. (c) Energy projection of the same cube gated by two γ rays: 385 keV in HPGe and 299 keV in $LaBr_3$:Ce.

it increases considerably the final uncertainty, reaching about 30%.

The lifetimes of excited states are extracted from the time difference between two γ rays observed in pairs of $LaBr_3$:Ce detectors. After all the corrections had been performed, data were sorted into $E_{\gamma 1}$-$E_{\gamma 2}$-ΔT cubes according to Ref. [22]. To further clean the cascade of interest detected in the $LaBr_3$:Ce detectors, additional γ rays detected in the HPGe are used as a gate. Figure 3 shows the effect of applying successive gates to the $E_{\gamma 1}$-$E_{\gamma 2}$-ΔT cube. This is illustrated for the 299–199 keV γ-ray cascade populating and deexciting the first 4^+ level at 287 keV. Figure 3(a) presents the HPGe-energy axis projection of a $\gamma\gamma\gamma$ (E_{HPGe}-E_{LaBr_3}-E_{LaBr_3}) coincidence cube. By gating on the 385 keV γ-ray in the HPGe detectors, the 299–199 keV cascade is selected [Fig. 3(b)]. The transition deexciting the level of interest can be seen in Fig. 3(c) where both gates (in HPGe and $LaBr_3$ detectors) have been applied.

Reference [22] describes two methods of extracting the lifetimes using the fast-timing technique. In the first method the lifetime is obtained by fitting the time distribution with an exponential function describing the law of radioactive decay convoluted with a Gaussian function representing the (prompt) time response distribution. For lifetimes comparable to or shorter than the time resolution of the $LaBr_3$:Ce detectors (which is typically between 100 and 300 ps) the centroid shift method can be applied. The lifetimes of excited states determined in the present paper cover a broad range, from ~1.5 ns to ~10 ps. Therefore, both methods have been employed. Figure 4 shows the time distributions extracted from the present experiment for excited states in the ground-state band up to the 6^+ state. The extracted lifetimes together with the corresponding reduced transition probabilities are given in Table II. The half-life for the first 2^+ state is found to be in good agreement with the previously measured value [$T_{1/2} = 1.49(4)$ ns] from Ref. [24]. The careful correction of

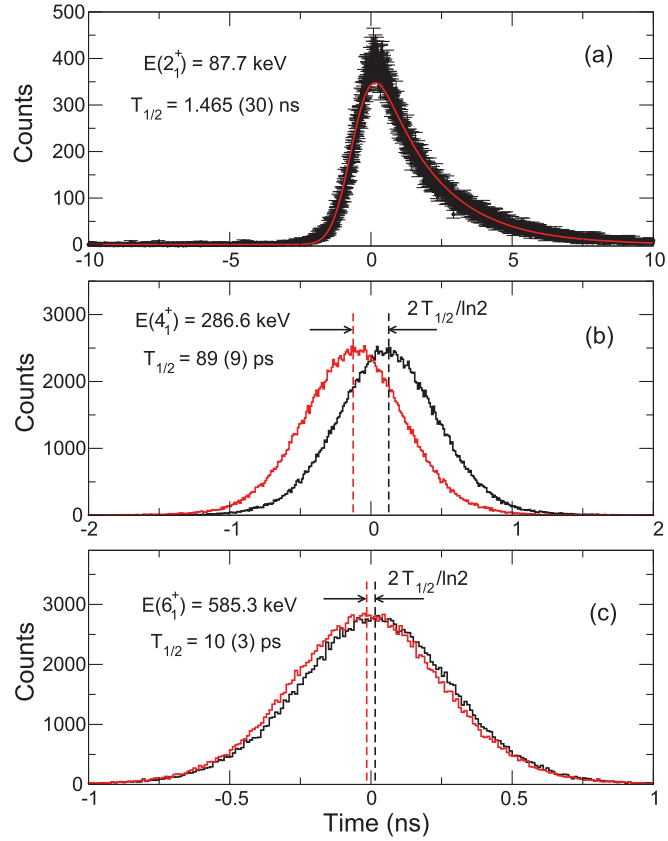

FIG. 4. (Color online) Time distributions for the 2^+ (a), 4^+ (b), and 6^+ (c) states in the ground-state band of ^{168}Yb. For the 2^+ state (a) the fit to the experimental data with the convoluted exponential decay function is presented (red line). For the other two states [(b) and (c)] the delayed coincidence time spectrum is obtained by considering the difference between the centroids of the distributions for $t_{start} - t_{stop}$ (black) and $t_{stop} - t_{start}$ (red).

the time walk performed for a large range of energies allowed the measurement of a half-life of ~10 ps, the shortest obtained so far with the in-beam fast-timing method [22]. Such a value is well within the range of usual plunger measurements, therefore allowing a future independent determination.

III. DISCUSSION

A. Positive-parity states

The positive-parity states were excited very strongly in this experiment. Therefore, several new levels and γ-ray

TABLE II. Half-lives for the 2^+, 4^+, and 6^+ states in the ground-state band obtained in the present experiment. The corresponding $B(E2)$ values for the $J_i \rightarrow J_f$ transitions are indicated.

E_{level} (keV)	J_i^π	K_i^π	$T_{1/2}$ (ps)	$B(E2; J_i \rightarrow J_i - 2)$ (W.u.)
87.73(1)	2_1^+	0_1^+	1465(30)	213(5)
286.55(2)	4_1^+	0_1^+	89(9)	290(30)
585.25(5)	6_1^+	0_1^+	10(3)	400(120)

transitions were found belonging to the β and γ bands. The spin assignments, especially for the β band where four new levels have been assigned, are made from the energy systematics of the levels in the neighboring nuclei.

1. Mikhailov branching ratios

An important characteristic of deformed nuclei is the presence of intraband $E2$ branching ratios that deviate from the Alaga rule. These deviations are considered to arise from a two-band mixing. The most studied case is that of γ–ground-state band mixing [25] which was systematically investigated in the rare-earth region and was found to exhibit a minimum at mid-shell. The easiest approach is to describe the mixing in the context of the Mikhailov plot formalism introduced in Ref. [26] and discussed in detail in Ref. [27]. It is interesting to perform such calculations to investigate whether the deviations from the Alaga rules observed in the present experiment can be explained by a two-state mixing formalism. If this is the case, we will then proceed to investigate whether more realistic models assuming axial symmetry are able to include the observed empirical deviations of these branching ratios from the simple rotational values. This is a crucial test of collective models.

In the small mixing amplitude approach and assuming that the mixing can be divided into a spin dependent and a spin independent part, one can define the modified $B(E2)$ values as [25]

$$\frac{\sqrt{B(E2; J_i \rightarrow J_f)}}{2\langle J_i K_i 2\Delta K | J_f 0\rangle} = M_1 - M_2[J_f(J_f+1) - J_i(J_i+1)], \tag{1}$$

where M_1 and M_2 are directly related to the unmixed transition matrix elements and the mixing amplitude. Therefore, we define

$$\rho_{\mathrm{exp}} = \frac{\sqrt{B(E2; J_i \rightarrow J_{f1})}/\langle J_i K_i 2\Delta K | J_{f1} 0\rangle}{\sqrt{B(E2; J_i \rightarrow J_{f2})}/\langle J_i K_i 2\Delta K | J_{f2} 0\rangle} \tag{2}$$

and

$$\rho_{\mathrm{calc}} = \frac{M_1 - M_2[J_{f1}(J_{f1}+1) - J_i(J_i+1)]}{M_1 - M_2[J_{f2}(J_{f2}+1) - J_i(J_i+1)]}, \tag{3}$$

the experimental and calculated Mikhailov branching ratios.

The most common indicators of the mixing are the parameters Z_β and Z_γ, for β- and γ-vibrational bands, respectively. They are related to the M_1 and M_2 parameters by [25–27]

$$Z_\beta = -\frac{M_2}{M_1}, \tag{4}$$

$$Z_\gamma = -\frac{2M_2}{M_1 + 4M_2}. \tag{5}$$

These parameters can be determined from interband corrected $E2$ branching ratios. The new transitions determined in the present experiments allow for a reliable deduction of the mixing with the yrast band. Using the $E2$ branching ratios of the 4^+ and 6^+ we have obtained $Z_\beta(4^+) = 0.0110(54)$ and $Z_\beta(6^+) = 0.0145(12)$, which agree within the error margins. For other states where both $M1$ and $E2$ transitions are possible no Z_β value has been extracted. The value for the 4^+ state has a very large uncertainty, therefore the value for the 6^+ state was preferred and used in all calculations. This value is considered to remain constant throughout the band. The mixing of the γ band with the yrast states was studied in a previous publication [2] and the parameters for the Mikhailov plot were obtained by considering the members between 2^+ and 5^+. The values reported are $\sqrt{2}M_1 = 0.406(15)$ eb and $\sqrt{2}M_2 = 0.0079(25)$ eb. The Mikhailov branching ratios together with the corresponding Alaga values are summarized in Table III. All experimental values are in good agreement with the calculated ones, indicating a rather successful explanation of the observed $B(E2)$ ratios by the two-state mixing approach. A large discrepancy appears only for the 2^+_β state which might indicate a more complex mixing. A similar analysis to the one performed in Ref. [25] would be very interesting as a future investigation for the β-vibrational band of the Yb isotopes. For the moment, this is beyond the scope of this paper.

TABLE III. Experimental and calculated (see text) Mikhailov branching ratios of the β- and γ-vibrational bands. The calculations are based on the assumption that all transitions are purely $E2$ and that Z_β and Z_γ remain constant. The errors of ρ_{exp} stem from the uncertainties of the transition intensities while the error of ρ_{calc} arises from the error of Z_β and Z_γ. Most of the values agree within the error margins.

E_{level} (keV)	J_i^π	J_{f1}^π	J_{f2}^π	ρ_{exp}	ρ_{calc}	Alaga
1233.1	2^+_β	2^+_1	0^+_1	0.45(28)[a]	1.10(14)	1.43
1390.03	4^+_β	6^+_1	4^+_1	0.95(42)	1.32(12)	1.75
	4^+_β	6^+_1	2^+_1	1.47(46)	1.65(14)	1.59
	4^+_β	4^+_1	2^+_1	1.55(37)	1.25(15)	0.91
1624.33	6^+_β	8^+_1	6^+_1	1.48(24)	1.43(11)	1.69
	6^+_β	6^+_1	4^+_1	1.42(15)	1.47(17)	0.81
1933.94	8^+_β	8^+_1	6^+_1	1.95(18)	1.77(19)	0.77
2309.76	10^+_β	10^+_1	8^+_1	3.55(15)	2.23(23)	0.74
2722.59	12^+_β	12^+_1	10^+_1	3.87(31)	3.00(30)	0.73
1445.00	6^+_γ	6^+_1	4^+_1	1.56(34)	1.75(43)	3.71
1618.32	7^+_γ	8^+_1	6^+_1	1.80(5)	1.80(25)	0.67
1792.82	8^+_γ	8^+_1	6^+_1	1.79(13)	2.40(109)	4.17

[a]Not excited in this experiment; taken from Ref. [2].

2. IBM and CBS calculations

While the two-state mixing formalism gives an idea about the validity of the rotational description, more detailed calculations are needed in order to understand the structure of ^{168}Yb and the systematic evolution of the whole isotopic chain. Therefore, calculations have been performed within the interacting boson model and the confined beta-soft rotor model, both approaches being very well suited to describe the structure of even-even deformed nuclei.

The interacting boson model was introduced by the work of Arima and Iachello [28], and it was proven to be a valuable tool in understanding the evolution of nuclear structure along isotopic chains [29]. To gain more insight into the detailed structure of Yb isotopes, calculations were performed in the IBM-1 framework (using s and d bosons) which makes no distinction between protons and neutrons. In the extended

consistent Q formalism, the Hamiltonian is written as

$$\hat{H}_{sd} = \epsilon \hat{n}_d + \kappa(\hat{Q} \cdot \hat{Q})^{(0)}, \tag{6}$$

where $\hat{Q}$ is the quadrupole operator given by

$$\hat{Q} = [(\hat{s}^{\dagger}\tilde{d} + \hat{d}^{\dagger}\hat{s})^{(2)} + \chi(\hat{d}^{\dagger}\tilde{d})^{(2)}] \tag{7}$$

and ϵ, κ, and χ are the model parameters.

The quadrupole electromagnetic transition operator is

$$\hat{T}(E2) = e_2 \hat{Q}, \tag{8}$$

where e_2 represents the boson effective charge [28].

The structure of each nucleus is defined by the competition between the three parameters in the Hamiltonian, ϵ, κ, and χ. These parameters are adjusted to fit the data in each nucleus, taking care at the same time to follow a smooth evolution of the parameters. For the nucleus ^{168}Yb, IBM calculations have been previously performed [13] and a direct comparison to the available experimental data has been shown. These calculations include data for Yb isotopes ranging from mass 158 to 172. Since there are some available experimental data concerning especially the positive-parity states in ^{174,176}Yb, we have extended the calculations in Ref. [13] keeping the same trend for the evolution of the parameters. The deduced values are $\zeta = 0.6$ and $\chi = -1.32$ for ^{174}Yb and $\zeta = 0.58$ and $\chi = -1.32$ for ^{176}Yb [ζ is defined in Ref. [13] as being $\zeta = 4N_B/(4N_B + \epsilon/\kappa)$]. For the present analysis we adopt these parameters together with those from Ref. [13] and use these calculations to investigate the agreement with the new experimental data. In the present experiments we have determined new branching ratios for the positive- and negative-parity states as well as some reduced transition probabilities for the yrast levels up to the 6^+ state. The negative-parity states will be discussed in the next section, so for the moment we concentrate the discussion only on the positive-parity states.

The most important feature of a nuclear structure model, besides its ability to reproduce all available experimental data, is the capability to predict reliable values for different observables. This is the reason why we have adopted a set of parameters which were fitted before the present results were known. The results of the IBM calculations for $E2$ transition probabilities are displayed in Fig. 5 [full line in panels (b), (d), and (f)] for all Yb isotopes ranging from mass 158 to 176, for which the reduced transitions probabilities between the low-lying states in the yrast band have been measured. The points in red are the values deduced in the present experiments, while the rest of the experimental data are taken from Refs. [30–38]. In addition we present also the experimental values of the lifetimes for the 2^+, 4^+, and 6^+ states in all Yb isotopes [panels (a), (c), and (e)], showing that our values are consistent with the systematic trends in this region. The calculations reproduce well the experimental trend, showing in general a slight overprediction for the reduced transition probability values in heavier nuclei. In these nuclei the hexadecapole degree of freedom might play an important role which is not included in the present version of the IBM. A better agreement was found in Ref. [12] where the g boson was also included at the cost of additional free parameters. From the trajectories in the IBM symmetry triangle found in Ref. [13], the structure of the Yb isotopes is

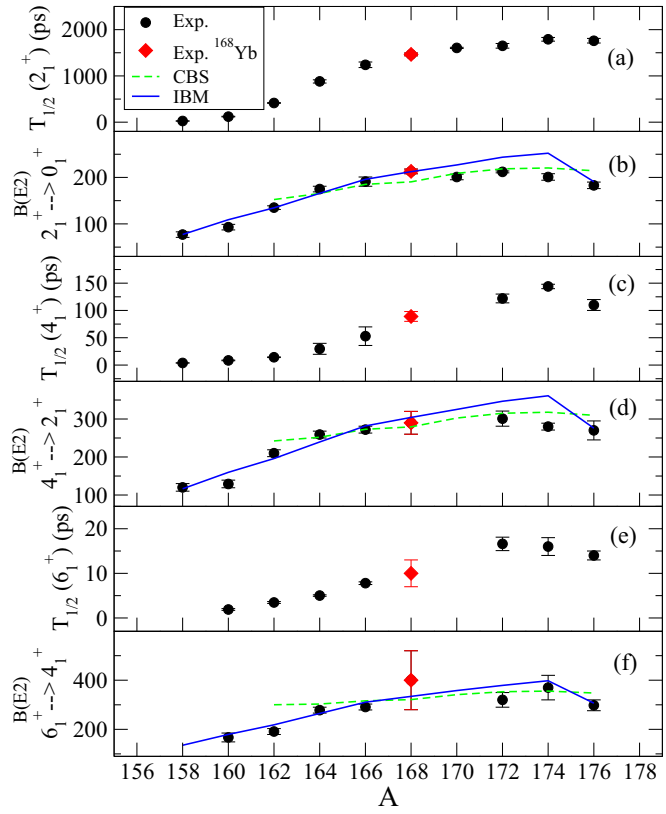

FIG. 5. (Color online) Experimental lifetimes [(a), (c), and (e)] and reduced $E2$ transition probabilities [(b), (d), and (f)] for the low-lying positive-parity states of the yrast band in Yb isotopes ranging from mass 158 to 176; points are experimental results, blue solid lines are IBM calculations, and green dashed lines are CBS calculations. The red points are the experimental values determined in the present experiments. The other experimental values are from Refs. [30–38]. The calculations reproduce well the experimental trend, showing in general a slight overprediction for the reduced transition probability values in heavier nuclei.

described as having an increased γ rigidity compared to the lower-Z nuclei in the same region while moving from the U(5) to the SU(3) leg of the symmetry triangle. In this picture ^{168}Yb is a transitional nucleus lying in the middle of the symmetry triangle.

Another nuclear structure model very well suited to study the rotational character of the transitional nuclei is the confined β-soft rotor model. After Iachello introduced the analytical solution for the X(5) critical point symmetry [39], the X(5) solution has been generalized by Pietralla and Gorbachenko [40] to an analytical solution describing the full transitional region between the critical point and the rigid rotor limit. The model was named the confined β-soft rotor model because it allows the β parameter to vary between two boundaries in order to parametrize the infinite-square-well potential. The model was used to predict the energies and transition probabilities for many deformed nuclei and showed its remarkable capability in describing the evolution of these observables [41].

Considering the Bohr Hamiltonian and assuming that the potential can be separated into β and γ parts, one obtains the

"radial" differential equation [40]

$$-\frac{\hbar^2}{2B}\left[\frac{1}{\beta^4}\frac{\partial}{\partial\beta}\beta^4\frac{\partial}{\partial\beta}-\frac{1}{3\beta^2}L(L+1)+u(\beta)\right]\xi(\beta)=E\xi_L(\beta), \tag{9}$$

where $u(\beta)$ is the infinite-square-well potential with boundaries at $\beta_M \geqslant \beta_m \geqslant 0$. The ratio $r_\beta = \beta_m/\beta_M$ parameterizes the width of the potential.

The quantization condition of the CBS rotor model is [40]

$$J_{\nu(L)}(z)Y_{\nu(L)}(r_\beta z) - J_{\nu(L)}(r_\beta z)Y_{\nu(L)}(z) = 0, \tag{10}$$

where J_ν and Y_ν are Bessel functions of first and second kind of irrational order $\nu(L) = \sqrt{L(L+1)/3+9/4}$. For a given parameter r_β and any spin value L the sth zero of Eq. (10) is denoted by $z_{L,s}^{r_\beta}$. Thus, the eigenvalues of Eq. (9) are obtained as [40]

$$E_{L,s} = \frac{\hbar^2}{2B\beta_M^2}\left(z_{L,s}^{r_\beta}\right)^2 \tag{11}$$

where $B\beta_M^2$ defines the energy scale.

Since we are interested to see how well the CBS rotor model can reproduce the experimental $B(E2)$ values, we define also the $E2$ transition operator, which takes the form [40]

$$T_\mu^{\Delta K=0}(E2) = e_{\rm eff}(\beta/\beta_M)D_{\mu 0}^2, \tag{12}$$

where $e_{\rm eff} = e^{(1)}\beta_M\langle cos\gamma\rangle_\gamma$ is the effective charge and D denotes the Wigner function.

Thus, the model provides three parameters to be adjusted to data: r_β and $B\beta_M^2$ for level energies and $e_{\rm eff}$ for transition probabilities. We have analyzed the ground-state bands up to 12_1^+ for energies and up to the highest known experimental value for $B(E2)$ values of all Yb isotopes with $R_{4/2} \geqslant 2.90$ (the value of the X(5) critical point symmetry). These are the Yb nuclei ranging from mass number 162 to 176. The effective charge was kept constant for the whole isotopic chain. The results for the transition probabilities are displayed in Fig. 5 (dashed line) and show in general a good agreement with the experimental data. A comparison of the relative moments of inertia produced by the CBS model with the experimental data for the ground state and for the β- and γ-vibrational bands will be given in the last section.

B. Negative-parity states

By comparison with the β- and γ-vibrational band members, octupole states were rather weakly excited in the present experiments. However, new transitions were observed which allowed some K quantum numbers to be assigned by comparison to the Alaga rule.

1. K quantum number assignment

In the unperturbed case, the ratio of the transition strengths connecting two intra- or interband transitions reduces to the ratio of the corresponding Clebsch-Gordan coefficients. This is usually referred to as Alaga rule [42].

Following this experiment, two negative-parity bands were proposed having assignments $K^\pi = 1^-$ ($J^\pi = 3^-$ at 1480 keV, $J^\pi = 4^-$ at 1597 keV, and $J^\pi = 5^-$ at 1770 keV) and $K^\pi = 2^-$ [$J^\pi = 4^-$ at 1650 keV, $J^\pi = (6^-)$ at 1842 keV, $J^\pi = (8^-)$ at 2100 keV, and $J^\pi = (10^-)$ at 2426 keV]. The reasons for these assignments are discussed next.

TABLE IV. $B(E1)$ ratios $R_{\rm exp} = \frac{B(E1;J_i^-\to(J_i+1)^+)}{B(E1;J_i^-\to(J_i-1)^+)}$ of octupole vibrational states compared to predictions of the Alaga rule for different possible K quantum number assignments.

$E_{\rm level}$ (keV)	J_i^π	K_f^π	$R_{\rm exp}$	R (Alaga rule)			
				$K_i^\pi = 0^-$	$K_i^\pi = 1^-$	$K_i^\pi = 2^-$	$K_i^\pi = 3^-$
1479.60	3^-	0_1^+	1.21(100)	1.33	0.75		
1650.19	4^-	2_γ^+	2.93(30)		5.60	1.40	0.11
1769.84	5^-	0_1^+	1.05(11)	1.20	0.83		
1842.08	6^-	2_γ^+	1.64(41)		3.09	1.21	0.24

Like in some other nuclei in this mass region, one negative-parity band (typically with $K^\pi = 2^-$) is established, which decays predominantly into the γ-vibrational band. This will be discussed in more detail in the next section and a comparison with the neighboring nuclei will also be shown. In the present experiments, a new transition of the state located at 1650 keV to the $J^\pi = 5_\gamma^+$ state was determined reducing the possible spins of this state to $(4)^-$. Furthermore, the transition of the (6^-) state at 1842 keV to the $J^\pi = (7_\gamma^+)$ state was observed. Using this new information the K quantum number was determined by a direct comparison with the Alaga rule. Table IV shows the predicted and the experimental values for the $B(E1)$ ratios for different possible K assignments. The states with $J^\pi = 4^-$ at 1650 keV and $J^\pi = 6^-$ at 1842 keV are closer to the Alaga prediction for a $K^\pi = 2^-$ band. Therefore, the whole band will be assigned to have $K^\pi = 2^-$ [43]. The 3^- state at 1479 keV and the 5^- state at 1770 keV show strong transitions to adjacent yrast spins suggesting a possible $K^\pi = 0^-$ or $K^\pi = 1^-$ assignment. A final decision based on the comparison with the Alaga rule cannot be made as the errors of the $B(E1)$ ratios are too large. However, the presence of the $J^\pi = 4^-$ at 1597 keV suggests a possible $K^\pi = 1^-$ assignment (even spins will not be allowed for a $K^\pi = 0^-$ band). Furthermore, a $K^\pi = 1^-$ value is favored if a mixing with the $K^\pi = 2^-$ band is assumed. This assumption is supported by the fact that the $J^\pi = 4^-$ state shows a weak decay to the γ-vibrational band which was observed in these experiments, but was too weakly excited to determine the corresponding branching ratio [43].

Two other states having $J^\pi = 5^-$ at 1999 keV and $J^\pi = (5,6,7)^-$ at 2111 keV are assigned to have $K \geqslant 2$ based on the multiple transitions to different bands for the first state and on the strong decay to the 1999 keV level for the latter [43].

2. Decay of the $K^\pi = 2^-$ band

As mentioned in the beginning of the previous section, the levels belonging to the negative-parity band denoted as $K^\pi = 2^-$ in ^{168}Yb show strong transitions to the γ-vibrational band as can be seen from the relative branching ratios in Table I. We notice, however, that this interesting behavior is not encountered only in ^{168}Yb, but it appears in most of the nuclei in this mass region. Systematics of the decay (branching ratios) of the octupole vibrational states decaying into the

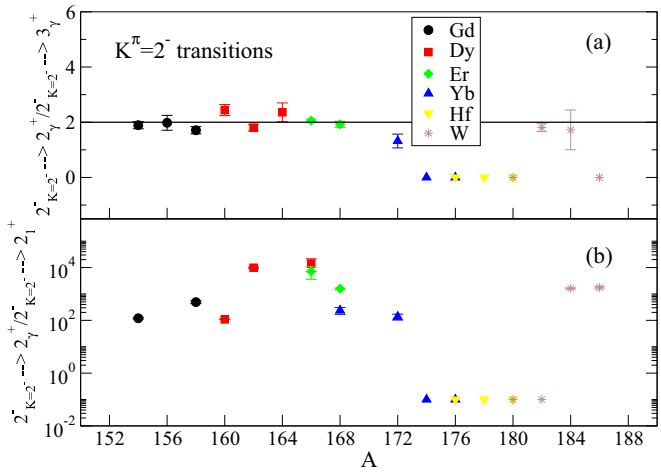

FIG. 6. (Color online) Systematic behavior of the branching ratios for the $J^{\pi} = 2^{-}$ state of the $K^{\pi} = 2^{-}$ octupole-vibrational band decaying only to the γ-band (a) or to the γ band and ground-state band for all nuclei between Gd ($Z = 64$) and W ($Z = 74$). A strong decay pattern is seen in two mass regions, for $A \leqslant 172$ and $A \geqslant 182$, and it stops abruptly in between. The data for ^{168}Yb in panel (b) corresponds to the $4^{-} \rightarrow 3^{+}_{\gamma}/4^{-} \rightarrow 4^{+}_{1}$ ratio. The solid line in panel (a) indicates the Alaga rule prediction for the corresponding transitions. The points in panel (b) with a branching ratio equal to zero are placed at 0.1 due to the logarithmic scale.

γ-vibrational band and into the ground-state band is shown in Fig. 6, where all nuclei between Gd ($Z = 64$) and W ($Z = 74$) have been searched. The experimental results have been taken from Refs. [19,30–38,44–50]. Because of the fact that the band head of the $K^{\pi} = 2^{-}$ band in ^{168}Yb was not populated in the present experiment and its decay is not known, we present in Fig. 6(b) the result for the decay of the 4^{-} state at 1650 keV to the γ band and to the ground-state band ($4^{-} \rightarrow 3^{+}_{\gamma}/4^{-} \rightarrow 4^{+}_{1}$). The results show that for most of the nuclei with $A \leqslant 172$ and $A \geqslant 182$ the $J^{\pi} = 2^{-}$ states belonging to the $K^{\pi} = 2^{-}$ band in each nucleus decay strongly into the γ-vibrational band when compared to the decay to the ground-state band [the decay to the ground state is weak, therefore the ratio in Fig. 6(b) is large]. This pattern stops abruptly between masses 172 and 182, the $K^{\pi} = 2^{-}$ states in these nuclei showing a strong decay to the $K^{\pi} = 0^{-}$ and $K^{\pi} = 1^{-}$ bands. This is exactly the region where the energy of the γ-vibrational band is increasing by about 500 keV. Although some of the $K^{\pi} = 2^{-}$ assignments may be questionable, it is very unlikely that the band members in all nuclei have in fact a different K quantum number. Therefore, this pattern seems to be important in the rare-earth region. Although this could indicate a possible octupole vibration on top of the gamma band, this would require knowledge of $E3$ strengths which are not available at this moment. We stress again the importance of additional experimental data for the negative-parity states in the rare-earth region.

3. *IBM-spdf calculations*

In the interacting boson model the positive-parity states are described by introducing s and d bosons with angular momenta $L = 0$ and $L = 2$, respectively. For the description of the negative-parity states one has to introduce additional bosons with odd values of angular momentum. After it was recognized that the addition of only the f bosons was not able to describe the $E1$ transition strengths, the p ($L = 1$) boson was also introduced and applied with success in Refs. [51–53]. Therefore, we adopt the IBM-$spdf$ framework for calculating the low-lying positive- and negative-parity states in ^{168}Yb.

The following Hamiltonian is used to describe simultaneously the positive- and negative-parity states

$$\hat{H}_{spdf} = \epsilon_d \hat{n}_d + \epsilon_p \hat{n}_p + \epsilon_f \hat{n}_f + \kappa(\hat{Q}_{spdf} \cdot \hat{Q}_{spdf})^{(0)}, \quad (13)$$

where ϵ_d, ϵ_p, and ϵ_f are the boson energies and $\hat{n}_p$, $\hat{n}_d$, and $\hat{n}_f$ are the boson number operators. In the $spdf$ model, the quadrupole operator is considered as being

$$\begin{aligned}\hat{Q}_{spdf} = \hat{Q}_{sd} + \hat{Q}_{pf} &= [(\hat{s}^{\dagger}\tilde{d} + \hat{d}^{\dagger}\hat{s})^{(2)} + \chi^{(sd)}(\hat{d}^{\dagger}\tilde{d})^{(2)}] \\ &+ \frac{3\sqrt{7}}{5}[(p^{\dagger}\tilde{f} + f^{\dagger}\tilde{p})]^{(2)} + \frac{9\sqrt{3}}{10}(p^{\dagger}\tilde{p})^{(2)} \\ &+ \frac{3\sqrt{42}}{10}(f^{\dagger}\tilde{f})^{(2)}. \end{aligned} \quad (14)$$

The quadrupole electromagnetic transition operator is:

$$\hat{T}(E2) = e_2 \hat{Q}_{spdf}, \quad (15)$$

where e_2 represents the boson effective charge.

For the $E1$ transitions there is more than one operator in the $spdf$ algebra. Consequently, a linear combination of the three allowed one-body interactions was taken:

$$\begin{aligned}\hat{T}(E1) = e_1\big[&\chi^{(1)}_{sp}(s^{\dagger}\tilde{p} + p^{\dagger}\tilde{s})^{(1)} + (p^{\dagger}\tilde{d} + d^{\dagger}\tilde{p})^{(1)} \\ &+ \chi^{(1)}_{df}(d^{\dagger}\tilde{f} + f^{\dagger}\tilde{d})^{(1)}\big], \end{aligned} \quad (16)$$

where e_1 is the effective charge for the $E1$ transitions and $\chi^{(1)}_{sp}$ and $\chi^{(1)}_{df}$ are two model parameters.

The calculations for the positive-parity states have been performed already in the previous section by using the parameters from Ref. [13]. Therefore, the same parameters are kept in the present calculations. For the description of the negative-parity states we allow up to three negative-parity bosons ($n_p + n_f = 3$). The only remaining parameters are then the p and f vibrational strengths which are set to $\epsilon_p = 1.5$ MeV and $\epsilon_f = 1.5$ MeV. The Hamiltonian in Eq. (13) conserves separately the number of positive- and negative-parity bosons and does not allow any admixtures of negative-parity bosons in the positive-parity states except for the presence of double dipole-octupole states (pairs of negative-parity bosons). Such states appear at higher energies and therefore the ground state and the β- and γ-vibrational states are not affected by the introduction of p and f bosons. The results obtained for these states in Ref. [13] remain exactly the same. Therefore in the following we will concentrate mainly on the discussion of the negative-parity states.

By employing the Hamiltonian from Eq. (13) we have observed that the ordering of the negative-parity bands with different K quantum number is not well reproduced. This means that the present Hamiltonian does not include a correct interaction. This situation can be improved by adding the

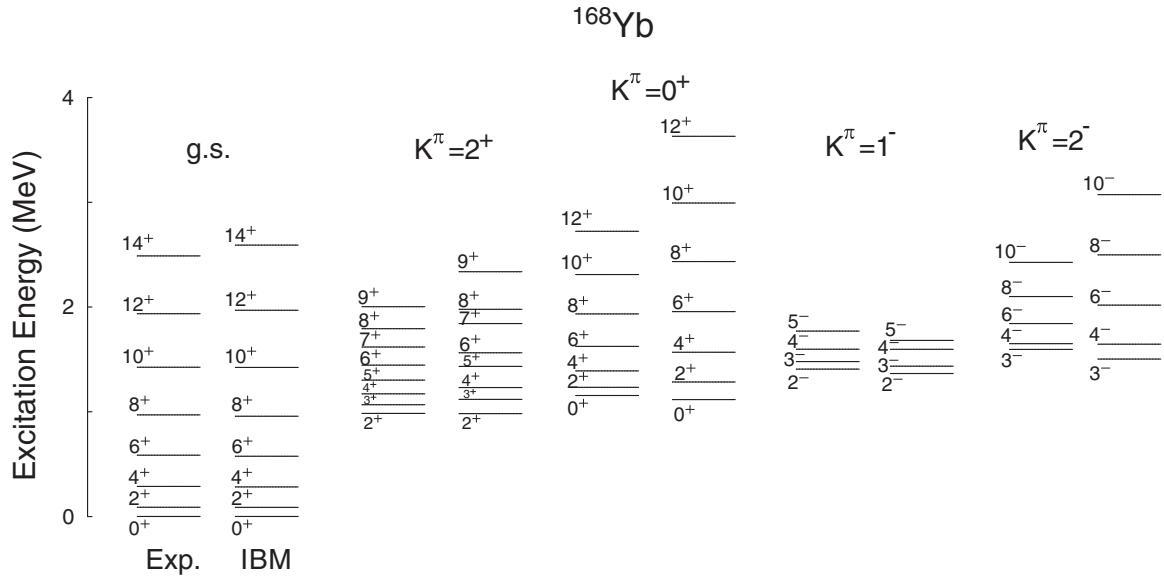

FIG. 7. Experimental excitation energies for the low-lying levels of ^{168}Yb in comparison with the present IBM-$spdf$ calculations. The states are grouped in bands and the ground-state band, the β- and the γ-bands (for the positive-parity states), and $K^\pi = 1^-$ and $K^\pi = 2^-$ bands (for the negative-parity states) are presented. The band heads for the octupole bands are not known experimentally and are therefore not included in the figure.

so-called "exchange term":

$$\hat{H} = \hat{H}_0 + a_3 \cdot 5 : (d^\dagger \tilde{f})^{(3)} \cdot (f^\dagger \tilde{d})^{(3)} : , \qquad (17)$$

where $\hat{H}_0$ is the Hamiltonian from Eq. (13). The importance of this term was explained in detail in Ref. [54] and was used to get the correct band ordering in the rare-earth region in the sdf-IBM framework. The value employed in the present paper for the strength of this term is $a_3 = -0.18$ MeV.

The quality of the present calculations in describing the experimental data can be observed in Fig. 7 where the calculated energy levels are compared to the corresponding low-lying available experimental data. The level energies of the ground-state band, γ- and β-vibrational bands, and those of the $K^\pi = 1^-$ and $K^\pi = 2^-$ bands are shown. The agreement for the energy levels is generally good. However, for the β-vibrational band and for the $K^\pi = 2^-$ band, the moment of inertia is overpredicted, resulting in rather large discrepancies between experimental values and calculated ones for high-spin states. This could be improved by introducing additional terms proportional to $\hat{L} \cdot \hat{L}$ in the Hamiltonian. These angular momentum terms will mostly affect the high-spin states. However, this will introduce additional parameters to be adjusted in the fit, while for the present calculations we try to keep the number of free parameters to the minimum.

For the positive-parity states, it is of interest to compare the relative centrifugal stretching of the ground-state, β-, and γ-vibrational bands to the CBS and IBM predictions. Similar to Ref. [55], we define the relative dynamical moment of inertia as

$$\frac{\theta_K(J)}{\theta_K(K+2)} = \left[\frac{J(J+1) - K(K+1)}{4K+6}\right] \times \frac{E(J=K+2) - E(K)}{E(J) - E(K)}. \qquad (18)$$

The results are presented in Fig. 8. The agreement for the ground-state band is rather good for both models, as shown in the upper graph of Fig. 8. However, the IBM model underestimates the moments of inertia at higher spins, showing a rather linear increase in contrast with experimental situation. Panel (b) shows the evolution of the relative moment of inertia for the β-vibrational band. The quantity which is plotted here is $\theta(J)/\theta(6)$ since no transition below 4^+_β was observed in the present experiment. The CBS model underestimates the values for $J = 0$ and $J = 2$ and gives a rather good description of the higher spin states. As stated in Ref. [55], this problem at low spin values may be due to small deviations from the square-well potential used in the CBS. This will have the greatest effect on low spin states. The IBM model gives a rather poor description of the data, as can be observed also from Fig. 7. This is due to the fact that the parameters of Ref. [13] were adopted for these calculations and they were fitted for the entire isotopic chain without taking into account the details of each nucleus. For the energies of the β band only the $E(0^+_2)/E(2^+_1)$ ratio was taken in the fit. The same rather poor reproduction of the data by the IBM model can be seen also in panel (c), where the relative moments of inertia as a function of spin for the γ-vibrational band are presented. The staggering given by the model is too large compared with the experimental values. Again, in fitting the parameters only the $E(2^+_\gamma)/E(2^+_1)$ ratio was taken into account. A fit of only ^{168}Yb would probably give a better reproduction of the experimental details. The agreement for the CBS is better, but this model fails to reproduce the staggering of the even/odd spin level energies. This staggering effect is believed to arise either from a band mixing of β- and γ-vibrational states or from weak γ fluctuations in the potential [56,57]. Both situations cannot be ruled out by the present data.

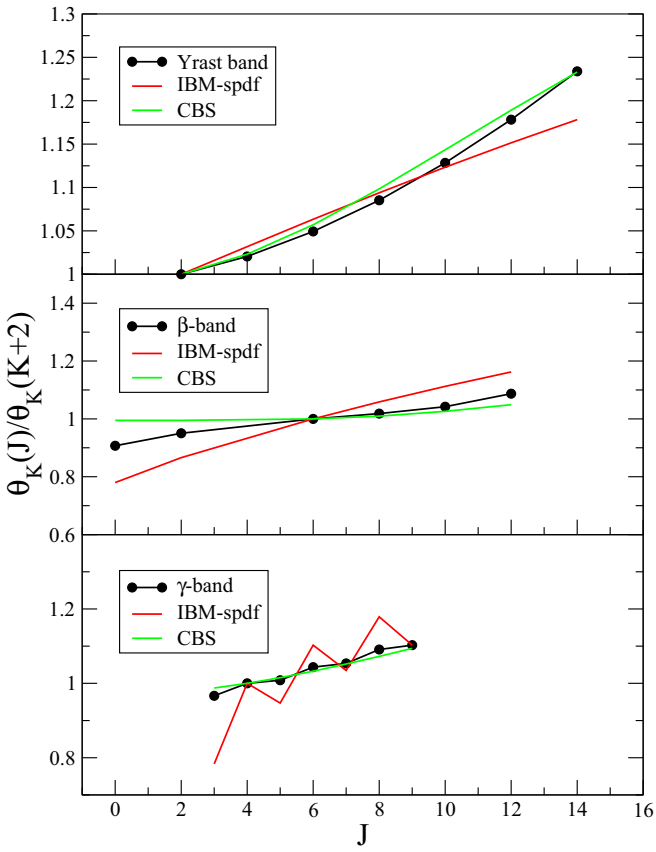

FIG. 8. (Color online) Evolution of the relative moment of inertia from Eq. (18) as a function of spin for the ground state band (a), β-vibrational band (b), and γ-vibrational band (c) with the predictions of IBM and CBS models.

A key point in describing the negative-parity states is the agreement between experimental and calculated $E1$ reduced transition probabilities. In ^{168}Yb there are no lifetimes measured for the negative-parity states, hence no absolute transition probabilities could be extracted. However, we can compare the calculated $E1$ ratios for the available data extracted from the present experiment. A detailed comparison between the experimental data and the present calculations is presented in Table V. The agreement is obtained by using $\chi_{sp} = -0.1$ and $\chi_{df} = 2.1$. With just a few exceptions, the calculations are in very good agreement with the experimental values, both for the $K^\pi = 1^-$ band and the $K^\pi = 2^-$ band. The IBM is particularly successful in reproducing the coupling to the γ-vibrational band of the states with $K^\pi = 2^-$.

IV. CONCLUSIONS

The nucleus ^{168}Yb was investigated via a fusion-evaporation reaction in two successive experiments. The strong population of the low-lying states enabled us to find new γ-ray transitions and to assign new levels. The β-vibrational band was considerably extended and the mixing with the yrast band was determined for the first time. The rather well established γ-vibrational band was extended by the $J^\pi = 8^+$ state and new decaying transitions were observed. For the negative-parity states, some new very weak transitions were seen and the K quantum number was determined from comparison to the Alaga rule. A very peculiar pattern of the $K = 2^-$ band strongly decaying into the γ-vibrational band is observed in ^{168}Yb similar to most of the nuclei below this mass number. The strong decay stops abruptly around mass 170 and is resumed around mass 180. Furthermore, the lifetimes of the yrast states up to 6^+ were determined by employing the in-beam fast-timing technique. The structure of ^{168}Yb is interpreted in terms of the IBM and CBS models, which show a good reproduction of the reduced transition strengths extracted from the present experiment and also for the whole isotopic chain. The negative-parity states have been calculated in the IBM-$spdf$ framework and show a good reproduction of the $B(E1)$ ratios from the $K^\pi = 1^-$ and $K^\pi = 2^-$ band to the yrast and γ-vibrational band.

TABLE V. Experimental and IBM-1 calculated $B(E1)$ ratios $\frac{B(E1;J_i^- \to J_{f1}^+)}{B(E1;J_i^- \to J_{f2}^+)}$ for states belonging to the $K^\pi = 1^-$ and $K^\pi = 2^-$ bands.

K_i^π	J_i^π	J_{f1}^π	J_{f2}^π	Expt.	Calc.
1^-	3_1^-	4_1^+	2_1^+	1.21(100)	1.10
	5_1^-	4_γ^+	4_1^+	0.80(31)	0.29
	5_1^-	6_1^+	4_1^+	1.05(11)	1.38
2^-	4_2^-	5_γ^+	3_γ^+	2.93(30)	5.72
	4_2^-	4_γ^+	3_γ^+	0.64(7)	1.06
	4_2^-	4_1^+	3_γ^+	0.0042(12)	0.0089
	6_2^-	7_γ^+	5_γ^+	1.64(41)	2.04
	6_2^-	6_γ^+	5_γ^+	0.45(12)	0.91
	6_2^-	6_1^+	5_γ^+	0.017(5)	0.59
	8_2^-	8_γ^+	7_γ^+	0.19(5)	0.84

ACKNOWLEDGMENTS

We greatly acknowledge the help of N. Pietralla, J. Beller, and M. Reese in providing and using the CBS code. This work has been supported by the Deutsche Forschungsgemeinschaft under Contract No. ZI 510/4-2 and by the Romanian Executive Unit for Financing Higher Education, Research, and Development, and Innovation (UEFISCDI) under contracts Crt. 127/F4 and PN-II-ID-PCE-2011-3-0367.

[1] A. Charvet, R. Chery, D. H. Phuoc, R. Duffait, A. Emsallem, and G. Marguier, Nucl. Phys. A **197**, 490 (1972).

[2] V. Barci, G. Ardisson, D. Trubert, and M. Hussonnois, Phys. Rev. C **60**, 024304 (1999).

[3] R. A. Meyer, D. R. Nethaway, A. L. Prindle, and R. P. Yaffe, Phys. Rev. C **35**, 1468 (1987).
[4] J. C. Bacelar *et al.*, Nucl. Phys. A **442**, 509 (1985).
[5] J. R. Oliveira *et al.*, Phys. Rev. C **47**, R926 (1993).
[6] A. Fitzpatrick *et al.*, Nucl. Phys. A **582**, 335 (1995).
[7] B. Elbek, M. Kregar, and P. Vedelsby, Nucl. Phys. A **86**, 385 (1966).
[8] M. A. Oothoudt and N. M. Hintz, Nucl. Phys. A **213**, 221 (1973).
[9] L. L. Riedinger, E. G. Funk, J. W. Mihelich, G. S. Schilling, A. E. Rainis, and R. N. Oehlberg, Phys. Rev. C **20**, 2170 (1979).
[10] S. W. Yates, T. B. Brown, C. D. Hannant, J. R. Vanhoy, and N. Warr, Acta Phys. Hung. N. S. **12**, 295 (2000).
[11] D. S. Chuu and S. T. Hsieh, J. Phys. G: Nucl. Part. Phys. **16**, 583 (1990).
[12] S. C. Li and S. Kuyucak, Nucl. Phys. A **604**, 305 (1996).
[13] E. A. McCutchan, N. V. Zamfir, and R. F. Casten, Phys. Rev. C **69**, 064306 (2004).
[14] N. Blasi, L. Guerro, A. Saltarelli, O. Wieland, and L. Fortunato, Phys. Rev. C **88**, 014318 (2013).
[15] H. Ganev, V. P. Garistov, and A. I. Georgieva, Phys. Rev. C **69**, 014305 (2004).
[16] J. Terasaki and J. Engel, Phys. Rev. C **84**, 014332 (2011).
[17] D. Ward *et al.*, Phys. Rev. C **66**, 024317 (2002).
[18] Y. Sun and J. L. Egido, Phys. Rev. C **50**, 1893 (1994).
[19] C. M. Baglin, Nucl. Data Sheets **111**, 1807 (2010).
[20] P. M. Walker, J. L. S. Carvalho, and F. M. Bernthal, Phys. Lett. B **116**, 393 (1982).
[21] J. N. Mo, R. Chapman, G. D. Dracoulis, W. Gelletly, and A. J. Hartley, Part. Nucl. **4**, 126 (1972).
[22] N. Mărginean *et al.*, Eur. Phys. J. A **46**, 329 (2010).
[23] J. M. Regis, Th. Matterna, G. Pascovici, S. Christen, A. Dewald, C. Fransen, J. Jolie, P. Petkov, and K. O. Zell, Nucl. Instrum. Methods Phys. Res. A **622**, 83 (2010).
[24] R. M. Ronningen, R. B. Piercey, J. H. Hamilton, C. F. Maguire, A. V. Ramayya, H. Kawakami, B. van Nooijen, R. S. Grantham, W. K. Dagenhart, and L. L. Riedinger, Phys. Rev. C **16**, 2218 (1977).
[25] R. F. Casten, D. D. Warner, and A. Aprahamian, Phys. Rev. C **28**, 894 (1983).
[26] V. M. Mikhailov, Izv. Akad. Nauk SSSR, Ser. Fiz. **28**, 308 (1964).
[27] A. Bohr and B. R. Mottelson, *Nuclear Structure, Vol. 2* (W. A. Benjamin, Reading, MA, 1969).
[28] F. Iachello and A. Arima, *The Interacting Boson Model* (Cambridge University Press, Cambridge, England, 1987).
[29] O. Scholten, F. Iachello, and A. Arima, Ann. Phys. (N.Y.) **115**, 325 (1978).
[30] R. G. Helmer, Nucl. Data Sheets **101**, 325 (2004).
[31] C. W. Reich, Nucl. Data Sheets **105**, 557 (2005).
[32] C. W. Reich, Nucl. Data Sheets **108**, 1807 (2007).
[33] B. Singh, Nucl. Data Sheets **93**, 243 (2001).
[34] C. M. Baglin, Nucl. Data Sheets **109**, 1103 (2008).
[35] C. M. Baglin, Nucl. Data Sheets **96**, 611 (2002).
[36] B. Singh, Nucl. Data Sheets **75**, 199 (1995).
[37] E. Browne and H. Junde, Nucl. Data Sheets **87**, 15 (1999).
[38] M. Basunia, Nucl. Data Sheets **107**, 791 (2006).
[39] F. Iachello, Phys. Rev. Lett. **87**, 052502 (2001).
[40] N. Pietralla and O. M. Gorbachenko, Phys. Rev. C **70**, 011304 (2004).
[41] K. Dusling and N. Pietralla, Phys. Rev. C **72**, 011303 (2005).
[42] G. Alaga, K. Alder, A. Bohr, and B. R. Mottelson, Mat. Fys. Medd. K. Dan. Vidensk. Selsk. **29**, 1 (1955).
[43] M. Elvers, Ph.D. thesis, University of Cologne, 2011 (unpublished).
[44] C. W. Reich, Nucl. Data Sheets **110**, 2257 (2009).
[45] C. W. Reich, Nucl. Data Sheets **113**, 2537 (2012).
[46] E. Achterberg, O. A. Capurro, and G. V. Marti, Nucl. Data Sheets **110**, 1473 (2009).
[47] S.-C. Wu and H. Niu, Nucl. Data Sheets **100**, 483 (2003).
[48] B. Singh and J. C. Roediger, Nucl. Data Sheets **111**, 2081 (2010).
[49] C. M. Baglin, Nucl. Data Sheets **111**, 275 (2010).
[50] C. M. Baglin, Nucl. Data Sheets **99**, 1 (2003).
[51] J. Engel and F. Iachello, Nucl. Phys. A **472**, 61 (1987).
[52] N. V. Zamfir and D. Kusnezov, Phys. Rev. C **63**, 054306 (2001).
[53] N. V. Zamfir and D. Kusnezov, Phys. Rev. C **67**, 014305 (2003).
[54] P. D. Cottle and N. V. Zamfir, Phys. Rev. C **54**, 176 (1996).
[55] K. Dusling *et al.*, Phys. Rev. C **73**, 014317 (2006).
[56] N. V. Zamfir and R. F. Casten, Phys. Lett. B **260**, 265 (1991).
[57] M. A. Caprio, Phys. Rev. C **72**, 054323 (2005).